

Nonlinear beam deflection in photonic lattices with negative defects

Jiandong Wang,¹ Zhuoyi Ye,² Alexandra Miller,³ Yi Hu,^{2,3} Cibo Lou,² Peng Zhang,³ Zhigang Chen,^{2,3} and Jianke Yang^{4,*}

¹College of Physical Electronics, University of Electronic Science and Technology of China, Chengdu 610054, China

²TEDA Applied Physical School, Nankai University, Tianjin 300457, China

³Department of Physics and Astronomy, San Francisco State University, San Francisco, California 94132, USA

⁴Department of Mathematics and Statistics, University of Vermont, Burlington, Vermont 05401, USA

(Received 7 February 2011; published 31 March 2011)

We demonstrate both theoretically and experimentally that a nonlinear beam can be reflected by a negative defect in a photonic lattice if the incident angle is below a threshold value. Above this threshold angle, the beam simply passes through the defect. This phenomenon occurs in both one- and two-dimensional photonic lattices, and it provides a way to use the incident angle to control beam propagation in a lattice network. If the defect is absent or positive, no evident transition from reflection to transmission occurs. These nonlinear phenomena are also compared with linear nondiffracting-beam propagation in a photonic lattice with a defect, and both similarities and differences are observed. In addition, some important features in linear and nonlinear beam propagations are explained analytically by using a linear model with a delta-function defect.

DOI: [10.1103/PhysRevA.83.033836](https://doi.org/10.1103/PhysRevA.83.033836)

PACS number(s): 42.65.Tg, 42.70.Qs

I. INTRODUCTION

Light propagation in waveguide arrays and photonic lattices has been attracting a lot of interest in recent years due to many novel effects exhibited by wave propagation in periodic structures. Examples include linear diffraction management, nonlinear light localization under self-focusing or self-defocusing nonlinearity, and light routing in lattice networks [1–4]. Light guiding by defects (or band-gap guidance) in waveguide arrays and photonic lattices has also been demonstrated both theoretically and experimentally [5–11]. In addition, recent experiments with laser-written waveguide arrays with structured defects or optically induced photonic lattices with tunable negative defects have led to the observation of two-dimensional (2D) defect surface solitons [12] as well as linear vortex defect modes [13]. Trapping of moving solitons by linear and nonlinear defects in a one-dimensional (1D) waveguide array has been proposed as well [14]. Very recently, localized defect modes have been observed with phase defects rather than amplitude defects in photonic structures [15,16]. In applications of photonic lattices for information processing, an important task is to identify mechanisms to change the propagation direction of light beams inside the lattice network. This problem has been investigated by having a soliton traveling in a specially designed lattice network or interacting with a blocker soliton [3,17–20]. In particular, it was shown that a weak (linear) probe beam launched at the zero-diffraction angle could be reflected by bright and dark soliton blockers [17,19].

In this article, we demonstrate both theoretically and experimentally that a nonlinear beam can be reflected by a negative (repulsive) defect in a photonic lattice if the beam's incident angle is below a threshold value. When the incident angle is above this threshold, the beam simply passes through the defect. Numerically, we find that the transition from reflection to transmission at the threshold angle is very sharp. Although precise experimental determination of such a

threshold angle poses a challenge, we clearly observe such a transition by varying the incident angle. This physical phenomenon provides a new way to use the incident angle to control the transmission or reflection of light beams in a lattice network. If the defect is absent or positive, no evident transition from reflection to transmission occurs; thus a negative defect is more robust for nonlinear beam control. These nonlinear beam dynamics are also compared with linear nondiffracting-beam propagation in a photonic lattice with a defect. It is found that the linear phenomena share some common features with the nonlinear phenomena. In particular, linear nondiffracting beams in lower Bloch bands, which move at smaller tilting angles, can be reflected by both positive and negative defects; but linear nondiffracting beams in higher Bloch bands, which move at larger tilting angles, can pass through these defects. By employing a delta-function defect model, many of these linear phenomena are analytically explained as well. Some differences between the linear and nonlinear phenomena also exist. In particular, nonlinear evolutions in uniform lattices and in lattices with positive defects at moderate incident angles are much more complex than the linear counterparts.

II. THEORETICAL STUDY OF BEAM PROPAGATION IN PHOTONIC LATTICES WITH DEFECTS

The theoretical model for beam propagation in a photonic lattice induced in a biased photorefractive nonlinear medium can be written as [2,9]

$$iU_z + U_{xx} + U_{yy} - \frac{E_0}{1 + I_L(x,y) + |U|^2} U = 0, \quad (1)$$

where U is the slowly varying amplitude of the probe beam, z is the direction of propagation (in units of $2k_0 n_e D^2 / \pi^2$), (x, y) defines the transverse plane (in units of D/π), E_0 is the applied dc field [in units of $\pi^2 / (k_0^2 n_e^4 D^2 r_{33})$], $I_L(x, y)$ is the photonic lattice with a single-site negative defect, and intensities of the probe beam and the lattice have been normalized by the dark irradiance of the crystal. Here D is the lattice spacing, $k_0 = 2\pi/\lambda_0$ is the wave number of the laser beam in the vacuum (λ_0 is the wavelength), n_e is the unperturbed

*jyang@cems.uvm.edu

refractive index, and r_{33} is the electro-optic coefficient for an extraordinary beam. In our experiments, the typical values of these physical parameters are $D = 30 \mu\text{m}$, $\lambda_0 = 0.5 \mu\text{m}$, $n_e = 2.3$, and $r_{33} = 280 \text{ pm V}^{-1}$. Thus, one (x, y) unit roughly corresponds to $10 \mu\text{m}$, one z unit roughly corresponds to 5 mm , and one E_0 unit roughly corresponds to 9 V mm^{-1} in physical units.

Our motivation for the present study is to explore new ways to control beam steering in a lattice network. For beam steering, an important requirement is that optical beams stay localized as they propagate through the lattice. If a beam propagates linearly (at low intensity, for instance), it will strongly diffract unless it is launched at the zero-diffraction angle [1,17,19]. This implies that there is no freedom to launch linear beams at arbitrary angles. On the other hand, it is well known that nonlinear beams can self-trap and form solitons in both homogeneous media and photonic lattices [1–4]. In addition, these solitons can be launched at a range of angles and still remain largely localized during propagation. This motivates us to explore how the incident angle affects nonlinear beam steering in photonic lattices, especially in the presence of a defect.

A. Nonlinear beam propagation in 1D case

First, we consider the 1D case, where Eq. (1) is y independent. In this case, we take the photonic lattice with a single-site defect as

$$I_L(x) = I_0 \cos^2 x [1 + h \exp(-x^8/128)], \quad (2)$$

where the lattice is π -periodic, its peak intensity is taken as $I_0 = 3$, the defect is confined to a single lattice site at $x = 0$, and h is the strength of the defect. When $h < 0$, the defect is negative (repulsive), while when $h > 0$, the defect is positive (attractive). These defected lattices with $h = -1$ and 1 as well as the uniform lattice (with $h = 0$) are shown in the first column of Fig. 1. The applied dc field in Eq. (1) is taken as $E_0 = 10$. The initial probe beam is taken as

$$U(x, 0) = r_0 e^{-(x-x_0)^2/2 + i\alpha x}, \quad (3)$$

with $r_0 = 3$, $x_0 = -2\pi$, which is a tilted Gaussian beam with peak intensity $r_0^2 = 9$ and is launched two lattice sites away from the defect site. The tilting angle of this Gaussian beam is proportional to the phase-gradient parameter α . Specifically, the physical tilting angle θ is related to α as

$$\theta = \alpha \lambda_0 / (2D), \quad (4)$$

where λ_0 is the beam's wavelength and D is the lattice spacing. At the typical experimental wavelength and lattice spacing mentioned earlier, this tilting angle is roughly equal to 0.008α radians, or 0.5α degrees. In our simulations, α is used as the control parameter. Note that without the lattice, this Gaussian beam (3) would form a soliton which moves at velocity 2α . Thus the power level of this Gaussian beam is in the nonlinear regime.

First, we consider the negative defect [$h = -1$ in Eq. (2)]. We find that when the incident angle is below a certain threshold (which is $\alpha_c \approx 1.23$ in the present situation), the beam is reflected back by the defect. These reflections at $\alpha = 0.94$ and 1.2 are displayed in Figs. 1(b) and 1(c), respectively

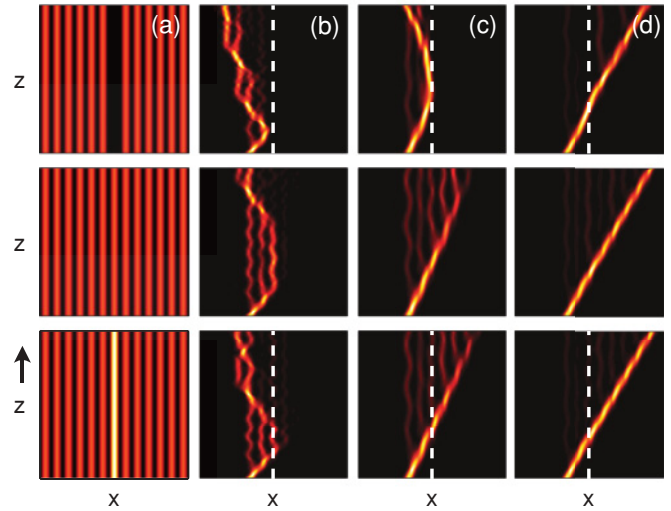


FIG. 1. (Color online) Nonlinear propagation of tilted Gaussian beams in a 1D lattice with a negative defect (top row), no defect (middle row), and a positive defect (bottom row). (a) Intensity field of the lattice; (b)–(d) beam evolutions at phase gradients $\alpha = 0.94$, 1.2 , and 1.5 , respectively. The simulation distance is $z = 20$ in (b) and $z = 8$ in (c) and (d). The vertical dashed lines mark the defect channel.

[note that the simulation distance is $z = 20$ in (b) and $z = 8$ in (c)]. However, above this threshold angle, the beam simply transmits through the defect. For instance, this transmission at $\alpha = 1.5$ is displayed in Fig. 1(d). For the physical parameters used above, this threshold α_c corresponds to a threshold tilting angle of $\theta_c \approx 0.6^\circ$.

What would happen if the defect is absent or positive? To address this question, we repeat the above simulations for these two cases (with all other parameters unchanged). The simulation results are displayed in the middle and lower rows of Fig. 1 for comparison. It is seen that for these two cases, the beam also transmits through the lattice or defect at large tilting angles [see Fig. 1(d)] and is reflected back at small tilting angles [see Fig. 1(b)], similar to the negative-defect case. However, at moderate angles, the beam largely passes through the lattice or defect in the uniform lattice and in the positive defect [see Fig. 1(c)], unlike the reflection in the negative defect. Thus, beam reflection near the threshold angle as shown in Fig. 1(c) results unambiguously from the negative defect.

To better understand beam propagations in the three lattices of Fig. 1(a), we now systematically investigate how the propagation outcome depends on the incident angle in these three cases. For this purpose, we perform a series of numerical simulations at many values of the phase gradient α . For each simulation, we monitor the percentage of the beam's energy that is reflected back. To measure this energy reflection, we define the reflection coefficient R as the ratio between the power of the beam on the left side of the defect ($x < -\pi/2$) and the total power of the beam at large propagation distances; i.e.,

$$R \equiv \frac{\int_{-\infty}^{-\pi/2} |U(x, z)|^2 dx}{\int_{-\infty}^{+\infty} |U(x, z)|^2 dx}, \quad z \gg 1. \quad (5)$$

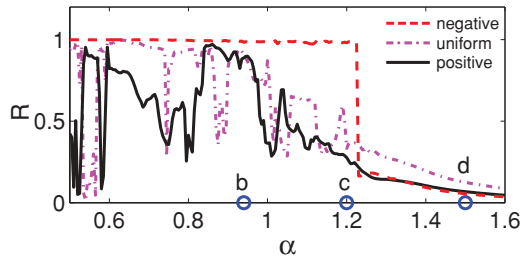


FIG. 2. (Color online) The reflection coefficients R versus the phase gradient α for the three lattices in column (a) of Fig. 1 (dashed red line for negative defect, dash-dotted pink line for uniform lattice, and solid black line for positive defect). The letters b, c, and d mark the values of the phase gradient α used in columns (b), (c), and (d) of Fig. 1.

Here the interval of $-\infty < x < -\pi/2$ is taken so that the energy trapped by the defect at $x = 0$ (if any) will not be counted as reflected energy. These reflection curves versus α for these three lattices are displayed in Fig. 2 (the simulation distance for this figure is $z = 20$). This figure shows that for all three lattices, the beam transmits through the defect or lattice at large tilting angles [such as $\alpha = 1.5$ of Fig. 1(d)]. At small tilting angles, however, outcomes for these three lattices show significant differences. In the negative defect, the beam is always reflected back when $\alpha < \alpha_c \approx 1.23$, and the transition from reflection to transmission at this threshold angle is very sharp. But in the uniform lattice and in the positive defect, the beam is reflected only for certain ranges of α values [such as $\alpha = 0.94$ of Fig. 1(b)], and is just partially reflected or not reflected at all for the other α values [such as $\alpha = 1.2$ of Fig. 1(c)]. In addition, the amount of reflected energy depends on α in a very complicated way. This intricate dependence of beam propagation on the tilting angle α may be related to resonant kink scattering by positive defects in the sine-Gordon and ϕ^4 models [21], but this question needs further investigation.

This angle-dependent beam reflection and transmission suggests a way to use the incident angle to control a beam's propagation direction inside a lattice network. For this application, the negative defect makes a good choice, because in this case the transition between reflection and transmission near the threshold angle is very sharp (see Fig. 2). For lattices with a positive defect and the uniform lattice, beam reflection is too sensitive to the incident angle, which may pose a challenge for engineering implementations.

It should be added that when the tilting angle is very small ($\alpha < 0.45$ in the present case), the beam will be trapped by its initial lattice site and unable to move across to the neighboring lattice sites. The reason for this trapping is that the photonic lattice creates a potential well at each lattice site. Since our probe beam is launched from the bottom of this potential well, if the tilting angle is very small, the beam cannot overcome this potential barrier and thus will be trapped in the initial lattice site.

B. Comparison with linear beam propagation in 1D

To understand the above nonlinear beam propagation in defects and uniform lattices, it is insightful to compare them

with linear beam propagation in the same situations. When the propagation is linear, due to lack of self-focusing, a narrow Gaussian beam such as (3) would strongly diffract and thus is not suitable for steering applications [1]. However, it is well known that Bloch bands of photonic lattices possess points of zero diffraction. When Bloch modes at these zero-diffraction points are modulated into localized packets and launched into the lattice, they can transmit through the lattice for long distances with little diffraction. These linear beams are often called nondiffracting beams, and their transmission angles are called nondiffracting angles. In the literature, it seems that only the nondiffracting beam in the first Bloch band was ever used [17,19], and its nondiffracting angle is relatively small. When this beam encounters bright and dark soliton blockers (which can be viewed as positive and negative defects), it was found to be reflected back by these blockers [17,19]. Below we will use nondiffracting beams not only on the first Bloch band but also on the higher bands. These linear beams will be launched into the lattices of Fig. 1(a). We will show that propagations of these linear beams share many features of the nonlinear beams in the previous subsection, but significant differences between them exist as well.

First, we illustrate these linear nondiffracting beams. In Fig. 3(a), the first Bloch band of the uniform lattice (with $h = 0$) is displayed. This Bloch band has two zero-diffraction points [where $\mu''(k) = 0$], and they are located at $k = \pm 0.55$. When the Bloch modes at these zero-diffraction points are modulated into localized packets, they would move across the lattice with little diffraction. This is illustrated in Fig. 3(b), where linear propagation of this nondiffracting beam at $k = 0.55$ in the uniform lattice is plotted. This figure is obtained by simulating the linear model of (1) (with the nonlinear term $|U|^2$ removed). The nondiffracting beam at $k = -0.55$

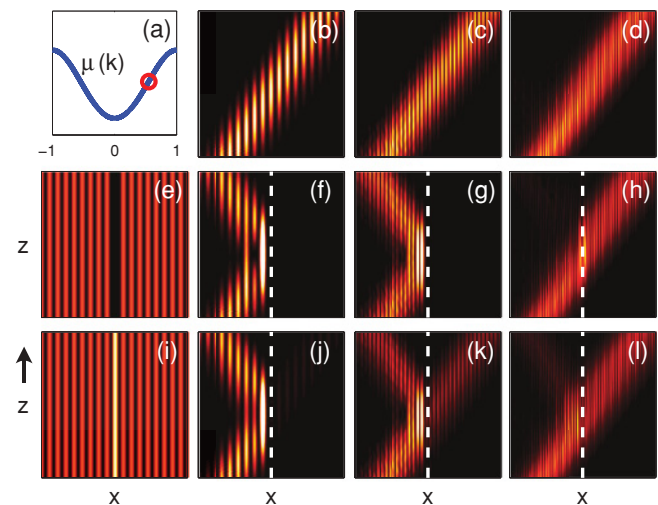


FIG. 3. (Color online) Linear propagations of nondiffracting beams in the uniform lattice (top row), with a negative defect (middle row), and with a positive defect (bottom row). (a) First Bloch band (the circle marks the zero-diffraction point); (e), (i) lattices with negative and positive defects. The second, third, and fourth columns show propagations of nondiffracting beams on the first, second, and third Bloch bands (with simulation distances $z = 120, 20$, and 8), respectively. The vertical dashed lines mark the defect channel.

has a negative tilting angle [$\mu'(k) < 0$] and is unnecessary to consider. On higher Bloch bands, zero-diffraction points exist as well. Specifically, these zero-diffraction points for the second and third Bloch bands are located at $k = 0.35$ and $k = 0.78$, respectively. Propagations of these nondiffracting beams on the second and third Bloch bands in the uniform lattice are displayed in Figs. 3(c) and 3(d). These figures confirm the “nondiffracting” nature of these beams. It should be noted that the evolution distances in Figs. 3(b), 3(c), and 3(d) are different. Specifically, these distances are $z = 120$, 20, and 8 for (b), (c), and (d), respectively. But their horizontal (x) axes are identical. Thus, Figs. 3(b)–3(d) show that the tilting angles of nondiffracting beams on the second and third Bloch bands are much larger than that on the first band.

Now, we launch these nondiffracting beams into the lattices with negative and positive defects [see column (a) of Fig. 1]. These lattices are reproduced in Figs. 3(e) and 3(i). Interactions of these nondiffracting beams with the defects are displayed in the second and third rows of Fig. 3. It is seen that the nondiffracting beam on the first Bloch band is reflected back by both the positive and negative defects [see Figs. 3(f) and 3(j)]. This result agrees with the previous ones reported in [17, 19]. However, the nondiffracting beam on the third band transmits through both the positive and negative defects [see Figs. 3(h) and 3(l)]. On the other hand, the nondiffracting beam on the second band is fully reflected by the negative defect [Fig. 3(g)] but is only partially reflected by the positive defect [Fig. 3(k)]. Recalling that the nondiffracting angles of these beams increase with higher Bloch bands, we see that the above linear propagations in defects resemble nonlinear ones in Fig. 1. In particular, for both linear and nonlinear propagations, the beam transmits through positive and negative defects at large tilting angles. At moderate tilting angles, the beam is reflected more strongly by negative defects than by positive defects. In addition, beam reflections in positive and negative defects at small tilting angles can occur in both linear and nonlinear systems. However, differences between linear and nonlinear propagations are also significant. One difference is that in a uniform lattice, a linear nondiffracting beam always transmits through the lattice [see Figs. 3(b)–3(d)], but a nonlinear beam could be reflected (see Fig. 1). Another difference is that nonlinear beams in uniform lattices and positive defects at small and moderate tilting angles exhibit much more complex evolution behaviors than linear nondiffracting beams (see Fig. 2).

C. Analysis of linear 1D phenomena using a delta-function defect model

The results in the above two subsections indicate that the linear model of (1) can capture many important features of nonlinear beam propagations. Thus we are motivated to analytically study this linear model so that a deeper understanding of these phenomena can be reached. In order to proceed analytically, we approximate the defect in (1) by a delta function, so that our linear 1D model equation becomes

$$iU_z + U_{xx} + [V(x) + H\delta(x)]U = 0, \quad (6)$$

where

$$V(x) = -E_0/(1 + I_0 \cos^2 x) \quad (7)$$

is a periodic potential, $\delta(x)$ is a delta defect function located at $x = 0$, and H is the strength of the delta defect ($H > 0$ for positive defect and $H < 0$ for negative defect). When the field is stationary, we can express the solution $U(x, z)$ of (6) as

$$U(x, z) = u(x)e^{-i\mu z}, \quad (8)$$

where μ is the propagation constant (in Bloch bands), and $u(x)$ is governed by the equation

$$u_{xx} + [V(x) - \mu + H\delta(x)]u = 0. \quad (9)$$

Without the defect, the solution to this linear equation is a combination of Bloch modes $u_1 = e^{ikx}p(x; k)$ and $u_2 = u_1^* = e^{-ikx}p^*(x; k)$, where k is the corresponding wave number of the propagation constant μ , $p(x; k)$ is a π -periodic function in x at wave number k , and the superscript $*$ represents complex conjugation. To simplify notations, we will suppress the k dependence of $p(x; k)$ and denote it just as $p(x)$ below.

In the presence of the delta defect, Eq. (9) defines a scattering problem, where

$$u(x) = \begin{cases} e^{ikx}p(x) + A e^{-ikx}p^*(x), & x < 0, \\ B e^{ikx}p(x), & x > 0. \end{cases} \quad (10)$$

Here $e^{ikx}p(x)$ at $x < 0$ is an incoming Bloch wave moving from $x = -\infty$ along the positive x axis, $A e^{-ikx}p^*(x)$ is the wave reflected by the defect and moves back to $x = -\infty$, $B e^{ikx}p(x)$ is the wave transmitted through the defect and moves to $x = +\infty$, and A, B are the amplitudes of reflected and transmitted waves, respectively. The values of A and B can be determined by the following conditions:

$$u(0^-) = u(0^+), \quad u'(0^-) - u'(0^+) = Hu(0). \quad (11)$$

The first condition of (11) is the continuity condition of $u(x)$ at $x = 0$. The second condition of (11) is the jump condition of $u'(x)$ at $x = 0$, which can be obtained by integrating Eq. (9) from $x = 0^-$ to 0^+ . Utilizing the two conditions in (11) as well as the formulas (10), we find that

$$A = -\frac{He^{i\rho}}{i\gamma + 2ik + H}, \quad B = \frac{i\gamma + 2ik}{i\gamma + 2ik + H}, \quad (12)$$

where

$$e^{i\rho} \equiv \frac{p(0)}{p^*(0)}, \quad \gamma \equiv 2 \operatorname{Im} \left(\frac{p'(0)}{p(0)} \right).$$

Here $\operatorname{Im}(\dots)$ represents the imaginary part of a complex number. It is easy to see that

$$|A|^2 + |B|^2 = 1, \quad (13)$$

which means that the sum of reflected and transmitted powers is equal to the power of the incoming wave. The percentage of reflected power in this scattering problem [i.e., the counterpart of the reflection coefficient defined in (5)] is

$$R = |A|^2 = \frac{H^2}{(\gamma + 2k)^2 + H^2}. \quad (14)$$

This formula shows that for delta defects, the amount of reflected power is always the same for positive and negative

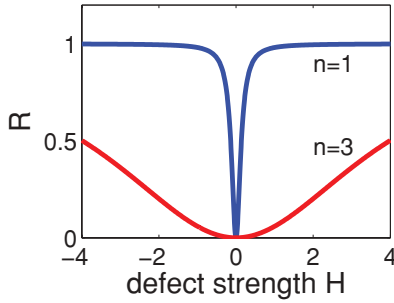


FIG. 4. (Color online) The reflection coefficients R versus the defect strength H for the nondiffracting beams on the first and third Bloch bands ($n = 1$ and $n = 3$) in the delta-defect model (6) with the periodic potential (7).

defects of the same strength $\pm H$. In addition, $R \rightarrow 0$ when $H \rightarrow 0$, and $R \rightarrow 1$ when $H \rightarrow \pm\infty$. In other words, if the defect is very weak, all energy will transmit through the defect, while if the defect is very strong, all energy will be reflected back by the defect. For a defect of moderate strength, the amount of reflected and transmitted powers will depend on the ratio $|\gamma + 2k|/|H|$ of the underlying Bloch wave. To illustrate, we take the periodic potential (7) which corresponds to the uniform lattice in Figs. 1 and 3 (with $E_0 = 10$ and $I_0 = 3$ as before). For the Bloch modes at the zero-diffraction points of the first and third bands (with $k = 0.55$ and 0.78 , respectively; see earlier text), we find that $\gamma = -0.9576$ for the former and $\gamma = 2.4236$ for the latter. The corresponding reflection coefficients R versus the defect strength H from formula (14) are plotted in Fig. 4. It is seen that at a moderate defect strength (say $H = \pm 1$), while the nondiffracting beam on the first Bloch band is mostly reflected back by the defect (since $|\gamma + 2k| = 0.1424 \ll |H|$), the nondiffracting beam on the third Bloch band mostly transmits through the defect (since $|\gamma + 2k| = 3.9836 \gg |H|$). These analytical results qualitatively explain the reflection of the first-band nondiffracting beam in Figs. 3(f) and 3(j) and transmission of the third-band nondiffracting beam in Figs. 3(h) and 3(l). Thus, the above analysis using a delta-function defect model deepens our understanding of linear beam propagations in lattices with defects. It should be pointed out, however, that not all analytical predictions from the above delta-defect model match the results of linear propagations in realistic defects [such as (2)]. For example, the above analysis predicts that the amount of power reflection is exactly the same for positive and negative defects of the same strength. This is not true for realistic defects [see Figs. 3(g) and 3(k)]. The reason for such discrepancies is our simplification of a realistic smooth defect by a single-point delta-function defect.

D. Nonlinear beam propagation in 2D case

We perform similar studies for beam deflection in 2D lattices, and find that results in the 2D case qualitatively resemble those in the 1D case (see Sec. II A). In this subsection, we focus on 2D beam propagations in a negative defect, since a negative defect is more feasible for beam-steering applications (see Fig. 2). For this purpose, we take the 2D lattice with a

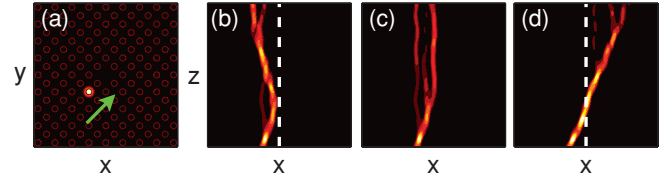


FIG. 5. (Color online) Nonlinear propagation of a tilted Gaussian beam in a 2D lattice with a negative defect. (a) The defected lattice and initial probe beam (its tilting direction is marked by an arrow); (b) beam reflection at a small incident angle (with defect); (c) propagation of the beam at the same incident angle of (b) in a perfect lattice (without defect); (d) beam transmission at a large incident angle (with defect). The vertical dashed lines mark the defect channel.

single-site negative defect as shown in Fig. 5(a), where the lattice is given by

$$I_L(x, y) = I_0 \cos^2 \frac{x+y}{\sqrt{2}} \cos^2 \frac{x-y}{\sqrt{2}} \{1 - e^{-(x^2+y^2)^4/128}\}, \quad (15)$$

with the peak intensity $I_0 = 3$ as in the 1D case. This lattice is oriented diagonally as in most experiments. The applied dc field is also $E_0 = 10$ as before, and the initial probe beam is a 2D Gaussian (with peak intensity 9) launched two sites away from the defect and tilted relative to the defect channel, as shown in Fig. 5(a). The simulation distance is $z = 10$. At small incident angles (specifically $\alpha < \alpha_c \approx 1.20$), the beam is also reflected. This is shown in Fig. 5(b) where the beam propagation in the (x, z) cross section is displayed. In this simulation, the tilting parameter $\alpha = 0.95$ is used. It is interesting to note that the threshold value $\alpha_c \approx 1.20$ in this 2D case is almost the same as the 1D threshold value $\alpha_c \approx 1.23$ in Sec. II A. Without this defect (i.e., in a perfect lattice), at the same small incident angle of Fig. 5(b), the beam would be split and trapped to nearby lattice sites, and no reflection occurs [see Fig. 5(c)]. Thus it is evident again that the negative defect leads to beam reflections, just like in the 1D case. At large angles ($\alpha > 1.20$), the beam passes the defect as shown in Fig. 5(d) (here $\alpha = 1.35$ is used).

III. EXPERIMENTAL RESULTS

The above predicted phenomenon has also been observed in our experiment. The experimental setup is similar to that used in our previous work with photonic defects [8,10]. The 1D lattice (spacing $32 \mu\text{m}$) with a single-site negative defect is created and maintained throughout the 11-mm-long photorefractive crystal at a bias field of 0.8 kV/cm [see Fig. 6(a)]. A tilted probe beam is launched into the lattice two sites away from the defect channel, as shown in Fig. 6(a). The probe beam is extraordinarily polarized, thus it undergoes strong nonlinear propagation in the biased crystal. At a small incident angle of about 0.5° , most of the probe beam is reflected by the defect channel when exiting the crystal [see Fig. 6(b)], but as the angle is increased to 0.76° , the probe beam passes through the defect [Fig. 6(d)]. In a perfect lattice under the same small launching angle of 0.5° as in Fig. 6(b), our experimental results show that beam reflection does not occur

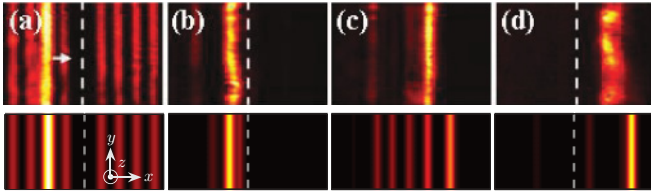


FIG. 6. (Color online) Experimental demonstration of beam reflection by a negative defect in a 1D lattice. (a) Transverse lattice pattern with a negative defect and input probe beam (brightest stripe) launched along z direction (pointing to the inside of the paper) but tilted toward the defect channel; (b) output (reflection) at a small incident angle (with defect); (c) output (transmission) at the same incident angle of (b) in a perfect lattice; (d) output (transmission) at a large incident angle (with defect). Top: experimental results; bottom: numerical results. White dashed lines mark the defect position.

[see Fig. 6(c)]. The bottom panels of Fig. 6 show our numerical simulation results. The numerical parameters are the same as in Fig. 1, except that the simulation distance is $z \approx 6$ here. Qualitative agreement between numerical and experimental results can be seen. Note that under current experimental conditions, the previously obtained theoretical threshold $\alpha_c \approx 1.23$ corresponds to a tilting angle $\theta_c \approx 0.55^\circ$ [see Eq. (4)]. Thus, the measured tilting angle for transition from reflection to transmission agrees well with the predicted threshold tilting angle, although precise experimental determination of such a threshold angle poses a challenge due to experimental reasons.

We also performed a series of experiments on beam reflection by a 2D negative defect, and typical results are shown in Fig. 7. In this experiment, a 2D lattice (spacing $40\mu\text{m}$) with a single-site negative defect is created and maintained throughout the 20-mm-long photorefractive crystal at a bias field of 2kV/cm [see Fig. 7(a)]. Similar to the 1D case, our probe beam is launched two sites away from the defect, as shown in Fig. 7(a). When the incident angle of the probe beam is about 0.46° , the probe beam is reflected by the defect channel [see Fig. 7(b)]. However, at the same angle but without defect, most of the probe beam tunnels through many lattice sites when exiting the crystal [see Fig. 7(c)]. In the presence of defect but when the probe beam is launched at a larger incident angle of about 0.7° , the probe beam again travels through many lattice sites with most of the power passing through the defect channel [see Fig. 7(d)]. Our corresponding numerical results from Fig. 5 are shown in the bottom panels of Fig. 7. Again, good qualitative agreement can be seen between the experimental results and numerical simulations. In addition, at the above experimental conditions, the theoretically obtained threshold $\alpha_c \approx 1.20$ in Sec. IID corresponds to a physical tilting angle $\theta_c \approx 0.43^\circ$. Experimentally, the observation is that if the angle

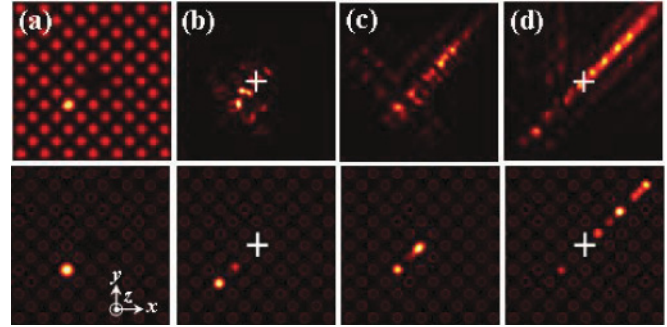


FIG. 7. (Color online) Experimental demonstration of beam reflection by a negative defect in a 2D lattice. (a) Defected lattice and input probe beam (brightest spot) launched along z direction but tilted diagonally toward the defect channel; (b) output (reflection) at a small incident angle; (c) output at the same incident angle of (b) when the defect is absent; (d) output (transmission) at a large incident angle. Top: experimental results; bottom: simulation results. The plus sign marks the defect location.

is smaller than 0.46° , most of the input beam is reflected by the defect. Otherwise, transmission dominates. Again, we have good agreement with the theoretical prediction.

IV. CONCLUSION

In summary, we have demonstrated both theoretically and experimentally that in a photonic lattice with a negative defect, a beam is reflected by the defect channel if the incident angle is below a threshold value. Above this threshold angle, the beam simply transmits through the defect. The transition from reflection-dominated propagation to transmission-dominated propagation near the threshold angle is evident in both numerical simulations and experimental observations. This phenomenon can be exploited to control beam propagation in a lattice network. If the defect is absent or positive, no sharp transition exists, and the beam's propagation depends on the incident angle in a more complex way. These nonlinear evolution phenomena have also been compared with linear nondiffracting-beam propagation in the same lattices, and both similarities and differences are found. In addition, some important features of linear and nonlinear propagations have been explained analytically by using a linear model with a delta-function defect.

ACKNOWLEDGMENTS

This work was supported by the National Science Foundation, the Air Force Office of Scientific Research, the 973 Program (2007CB613203), the National Natural Science Foundation of China, and the Changjiang Scholars Program.

- [1] H. S. Eisenberg, Y. Silberberg, R. Morandotti, A. R. Boyd, and J. S. Aitchison, *Phys. Rev. Lett.* **81**, 3383 (1998).
 [2] J. W. Fleischer, M. Segev, N. K. Efremidis, and D. N. Christodoulides, *Nature (London)* **422**, 147 (2003).

- [3] D. N. Christodoulides and E. D. Eugenieva, *Phys. Rev. Lett.* **87**, 233901 (2001).
 [4] R. Fischer, D. Trager, D. N. Neshev, A. A. Sukhorukov, W. Krolikowski, C. Denz, and Y. S. Kivshar, *Phys. Rev. Lett.* **96**, 023905 (2006).

- [5] U. Peschel, R. Morandotti, J. S. Aitchison, H. S. Eisenberg, and Y. Silberberg, *Appl. Phys. Lett.* **75**, 1348 (1999).
- [6] H. Trompeter, U. Peschel, T. Pertsch, F. Lederer, U. Streppel, D. Michaelis, and A. Bräuer, *Opt. Express* **11**, 3404 (2003).
- [7] F. Fedele, J. Yang, and Z. Chen, *Opt. Lett.* **30**, 1506 (2005).
- [8] I. Makasyuk, Z. Chen, and J. Yang, *Phys. Rev. Lett.* **96**, 223903 (2006).
- [9] J. Yang and Z. Chen, *Phys. Rev. E* **73**, 026609 (2006).
- [10] X. Wang, J. Young, Z. Chen, and J. Yang, *Opt. Express* **14**, 7362 (2006).
- [11] J. Yang, X. Wang, J. Wang, and Z. Chen, in *Nonlinearities in Periodic Structures and Metamaterials*, edited by C. Denz, S. Flach, and Y. S. Kivshar (Springer, Berlin, 2009), pp. 127–143.
- [12] A. Szameit, Y. V. Kartashov, M. Heinrich, F. Dreisow, T. Pertsch, S. Nolte, A. Tünnermann, F. Lederer, V. A. Vysloukh, and L. Torner, *Opt. Lett.* **34**, 797 (2009).
- [13] D. Song, X. Wang, D. Shuldman, J. Wang, L. Tang, C. Lou, J. Xu, J. Yang, and Z. Chen, *Opt. Lett.* **35**, 2106 (2010).
- [14] L. Morales-Molina and R. A. Vicencio, *Opt. Lett.* **31**, 966 (2006).
- [15] A. Szameit, M. I. Molina, M. Heinrich, F. Dreisow, R. Keil, S. Nolte, and Y. S. Kivshar, *Opt. Lett.* **35**, 2738 (2010).
- [16] P. P. Belicev, I. Ilic, M. Stepic, A. Maluckov, Y. Tan, and F. Chen, *Opt. Lett.* **35**, 3099 (2010).
- [17] J. Meier, G. I. Stegeman, D. N. Christodoulides, Y. Silberberg, H. Yang, G. Salamo, M. Sorel, and J. S. Aitchison, *Opt. Lett.* **30**, 1027 (2005).
- [18] J. Meier, G. I. Stegeman, D. N. Christodoulides, R. Morandotti, G. Salamo, H. Yang, M. Sorel, Y. Silberberg, and J. S. Aitchison, *Opt. Lett.* **30**, 3174 (2005).
- [19] E. Smirnov, C. E. Ruter, M. Stepic, V. Shandarov, and D. Kip, *Opt. Express* **14**, 11248 (2006).
- [20] X. Wang and Z. Chen, *Opt. Express* **17**, 16927 (2009).
- [21] Y. S. Kivshar, Z. Fei, and L. Vázquez, *Phys. Rev. Lett.* **67**, 1177 (1991).